GEOPHYSICAL RESEARCH LETTERS, VOL. 26, NO. 22, PAGES 3357-3360, NOVEMBER 15, 1999

# Ionization of the Lower Ionosphere by $\gamma$–rays from a Magnetar: Detection of a Low Energy (3–10 keV) Component

U. S. Inan, N. G. Lehtinen, S. J. Lev-Tov, M. P. Johnson, T. F. Bell

STAR Laboratory, Stanford University, Stanford, CA 94305

K. Hurley

UC Berkeley Space Sciences Laboratory, Berkeley, CA 94720-7450

**Abstract.** A gigantic periodic flare from the soft $\gamma$ repeater SGR 1900+14 produced enhanced ionization at ionospheric altitudes of 30 to 90 km, which was observed as unusually large amplitude and phase changes of very low frequency (VLF) signals propagating in the Earth-ionosphere waveguide. The VLF signals remained perturbed for ~5 min and exhibited the 5.16 s periodicity of the giant flare detected on the Ulysses spacecraft [*Hurley et al.*, 1999]. Quantitative analysis indicates the presence of an intense initial low energy (3–10 keV) photon component that was not detectable by the Ulysses instrument.

## 1. Introduction

VLF remote sensing is a sensitive means for probing the lower ionosphere (~40 to 90 km altitude), used to measure solar X-ray flares and sporadic electron precipitation due to magnetospheric disturbances and aurorae [see references in *Fishman and Inan*, 1988 and *Cummer et al.*, 1997], lightning-induced electron precipitation out of the radiaton belts [e.g., *Inan and Carpenter*, 1987], and direct disturbances of the lower-ionosphere by lightning [*Inan et al.*, 1996].

The possibility of detectable ionospheric effects of celestial X-ray sources [*Edwards et al.*, 1969] was pursued by rocket-based [*Goldberg et al.*, 1985] and VLF methods [see references 19–24 in *Fishman and Inan*, 1988] leading to the observation of an ionospheric disturbance caused by a $\gamma$–ray burst [*Fishman and Inan*, 1988].

On August 27th, 1998, at ~3:22 PDT (10:22 UT), an extremely intense hard X-ray/$\gamma$–ray flare ionized the exposed part of the Earth's nightside lower ionosphere, producing ionization levels usually found only during daytime. The flare originated from a neutron star, located some 23,000 light years away, known as Soft Gamma Repeater (SGR) 1900+14, also believed to be a 'magnetar' [*Hurley et al.*, 1999]. The giant flare lasted for ~5 min, and exhibited strong fluctuations at a rate of 5.16 s, the period of rotation of the magnetar. The photon-flux-time-energy distribution in the 20–150 keV range was measured by instruments on Ulysses, which were not sensitive to lower energy photons. The intense burst of energetic photons produced enhanced ionization at ionospheric altitudes of 30 to 90 km, observed as unusually large VLF signal changes, lasting for ~5 min and exhibiting a 5.16 s fluctuation. Comparison of the VLF data with predictions of a quantitative model of enhanced ionization and its effects on subionospheric VLF signals indicate that the giant flare, observed in ~20-150 keV photons by Ulysses, was in fact accompanied by a significant low energy (3–10 keV) photon component.



Paper number 1999GL010690.
0094-8276/99/1999GL001069005.00

## 2. Observations

Figure 1a shows the earth's ionosphere exposed to the giant flare and the VLF signal paths from the 21.4 kHz transmitter in Hawaii, known by its call sign "NPM", to Palmer Station, Antarctica (PA), to Boston (BO), and nine sites constituting the Holographic Array for Ionospheric Lightning (HAIL) at which amplitude and phase of the NPM signal were recorded by Stanford receivers with 20-ms resolution.

Figure 1b shows the typical relatively low daytime levels of the NPM–HAIL signal followed by increased but highly variable nighttime levels, with perturbations of $\Delta A > 0.2$ dB being typical of lightning-induced disturbances [*Inan et al.*, 1996]. The giant flare produces a ~15 dB change, driving the signal to its low daytime levels. The sudden onset and the recovery of the VLF event (Figure 1c) tracks the profile of the giant flare (Figure 1d). No effects were observed on VLF signals arriving at HAIL from the east, propagating through the unexposed ionosphere.

The event was also observed (Figure 2) on the NPM–PA and NPM–BO signals, with the NPM–PA signal change exhibiting unprecedented size ($\Delta A \simeq 20$ dB, $\Delta\phi \simeq 65°$) and 'sudden' onset (<20 ms). The event onset was so rapid and intense that the phase-locked loop first lost and then regained lock so that $\Delta\phi \simeq 65°$ is a lower bound. The first hint of the sudden arrival of the giant flare was observed on Ulysses (Figure 3a) at 39241.661 s UT (1023:01.661 s UT), corresponding to flare impact at the sub–SGR1900 point of 1022:15.603 s UT, compared to the event onset at Palmer of 1022:15.671 s UT (Figure 3b). The ~70 ms difference is consistent with the distance between the sub–SGR1900 point and the NPM–PA path, and the propagation of the perturbation onset to Palmer. The NPM–PA signal change occurs within one data sample (<20 ms), while the Ulysses data (~30 ms resolution) shows an onset duration of ~60 ms (Figure 3a). Absolute accuracy of the VLF data is <1 ms, while that of the Ulysses data is several ms.

The 5.16 s pulsations exhibited by the giant flare after about 1023 UT (see Figure 1d) are weakly evident on the NPM–PA signal (Figure 4a) and are also revealed by spectral analysis of the NPM–HAIL data (Figure 4b).

## 3. Interpretation

**$\gamma$–ray Penetration Into the Atmosphere.** A Monte Carlo model using $10^7$ photons was constructed to calculate

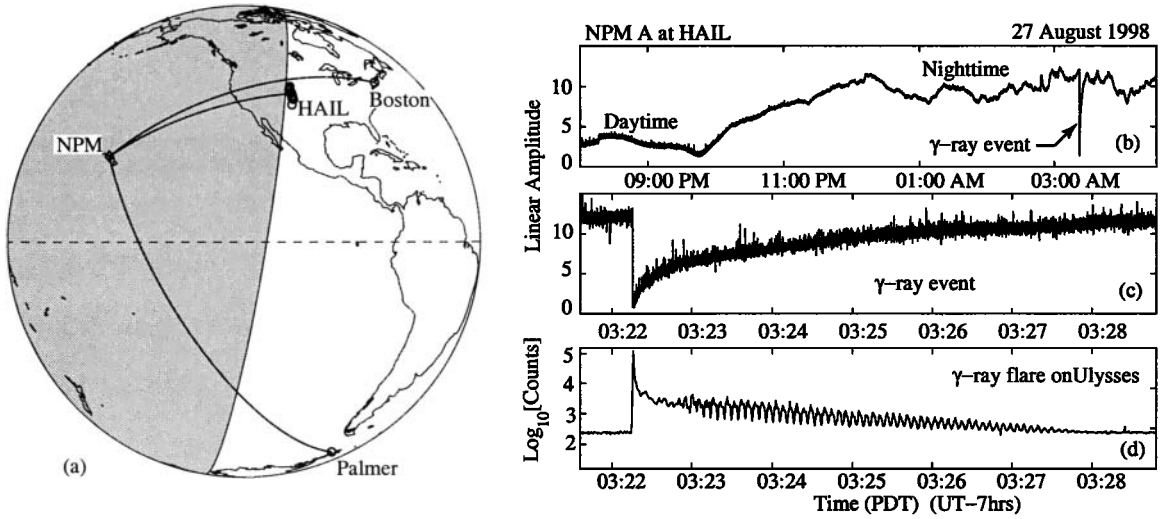


**Figure 1.** (a) The VLF great-circle paths from the NPM transmitter to Boston, Palmer, and the HAIL network. The part of the globe illuminated by the γ–ray flare is indicated by shading. (b) The amplitude of the 21.4 kHz NPM signal observed in Trinidad, Colorado. (c) Expanded record of the γ–ray flare event which occurs at ~3:22 am PDT. (d) The intensity of the giant flare observed on Ulysses (from [*Hurley et al.*, 1999]).

the energy deposition and ionization by the γ–rays incident on the upper atmosphere [*Fano et al.*, 1959]. We used published data on photon cross sections, attenuation, and energy absorption coefficients [*Hubbell*, 1969; *Storm and Israel*, 1970] and accounted for Compton scattering of photons by electrons [using the Klein-Nishina formula, eq. 41 from p. 219 of *Heitler*, 1954], and the absorption of a photon as it removes an electron from its shell (photoeffect), including relativistic [eq. 17 from p. 209 of *Heitler*, 1954] as well as absorption edge effects [eq. 16 from p. 208 of *Heitler*, 1954]. Rayleigh scattering at small angles (much smaller cross section compared to Compton effect), and pair production (maximum photon energy of ~240 keV is smaller than twice the electron rest energy) were neglected.

Since the Compton electrons do not produce much bremsstrahlung the photons are considered one-by-one using time steps equal to the time between successive collisions. Starting with an initial photon flux-energy-time distribution incident at 150 km at a zenith angle $\psi$, we calculate the energy deposition by assuming [*Brown*, 1973] that all energy lost by a photon is deposited by the Compton electron within 1 km of the point of its production. The secondary electron production rate is then determined by using the mean energy loss per ion pair formed of 35 eV [*Rees*, 1963]. For Compton scattering, only a portion of the photon energy is deposited at the point of collision, whereas in the photoeffect, all photon energy is deposited locally. Our Monte Carlo model results agree well with past calculations of ionization profiles expected from γ–rays incident on the atmosphere [see references 23, 26, and 28–30 in *Fishman and Inan*, 1988].

Time-evolution of electron density $N_e$ is calculated using a four-constituent (electrons, positive and negative ions, and positive cluster ions) model [*Pasko and Inan*, 1994, and references therein], with the effective coefficient of dissociative recombination $\alpha_d \simeq 6 \times 10^{-7}$ cm$^3$ s$^{-1}$, and assuming negligible electron detachment.

The incident flux-energy-time distribution is determined from Ulysses data [*Hurley et al.*, 1999]. An energy distribution of $f(\mathcal{E}) = [\Phi_E/(\mathcal{E}T)]e^{-\mathcal{E}/T}$, where $\Phi_E$ is the total energy flux, and $T$ is the photon temperature, provides a good fit to the detected particle flux in the 22 to 149 keV range of the instrument for $T = 200$ keV during the initial second of the giant flare and for $T = 30$ keV after the first second.

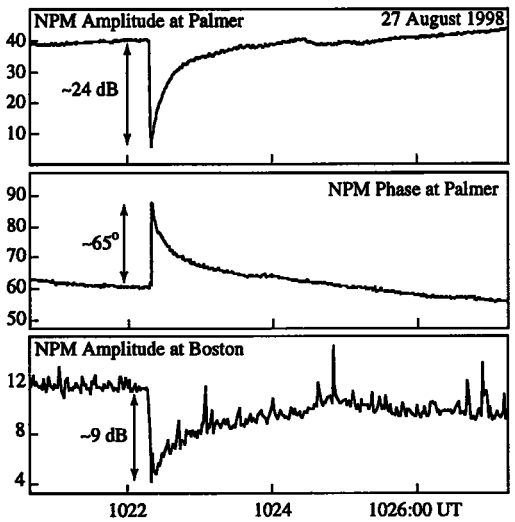


**Figure 2.** Top two panels: NPM signal amplitude and phase observed at Palmer. Bottom panel: NPM signal amplitude at Boston.

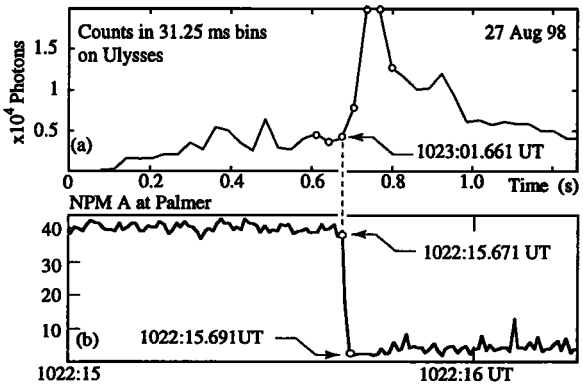


**Figure 3.** (a) Photon counts per 31.25 ms time bins observed on Ulysses. (b) NPM signal amplitude observed at Palmer.

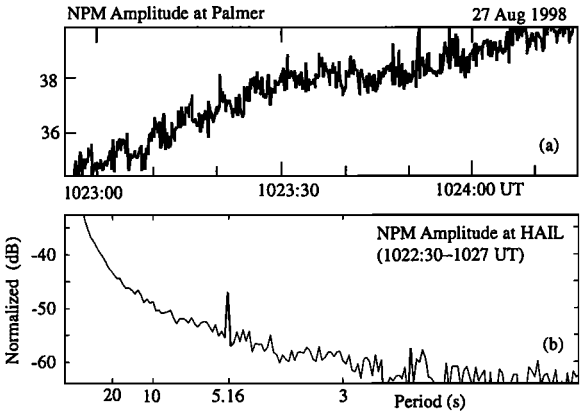


**Figure 4.** (a) The NPM–PA signal during the period when 5.16 s oscillation was exhibited by the $\gamma$–ray flare (Figure 1d). (b) The frequency spectrum of the NPM–HAIL amplitude plotted versus period.

Calculated profiles for electron density $N_e$ and conductivity $\sigma$ corresponding to different time instants are shown in Figure 5a and 5b for $\psi = 60°$, and for a typical ambient nighttime $N_e$ profile [*Lev-Tov et al.*, 1996]. Here, the conductivity $\sigma = \sigma_{ion} + \sigma_{elec}$, where only $\sigma_{elec}$ is modified by the enhanced $N_e$. Due to the high electron-neutral collision rate, $\sigma_{ion}$ is dominant for $< 60$ km, where $\Delta\sigma \simeq 0$, in spite of enhanced $N_e$. The $N_e$ and $\sigma$ at 80 km and 70 km (Figure 6a and 6b) continue to increase for ~50 s following the onset of the flare, unlike the observed sharp VLF changes (Figure 3b). The 5.16 s pulsations are evident at 70 km (Figure 6c), but not at 80 km, due to the slower recombination rate. Both Figures 5b and 6a,c indicate that the $\Delta\sigma$ are quite small compared to the difference between daytime and nighttime ambients, basically due to the fact that the >20 keV photons deposit their energy at <60 km. In addition, both $N_e$ and $\sigma$ recover back to ambient levels in >300 s compared to the <200 s recovery of the VLF changes.

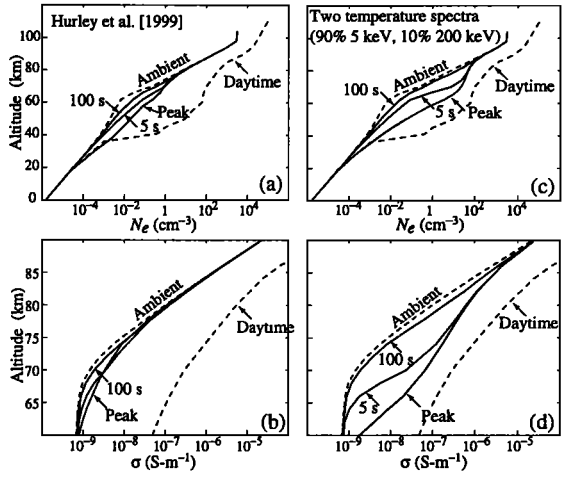


**Figure 5.** (a) Altitude profile of $N_e$, before (Ambient), immediately after (Peak), 5 s, and 100 s after the onset of the giant flare, calculated with a Monte Carlo model, for the photon flux-energy-time distribution given by *Hurley et al.*, 1999] and for $\psi = 60°$. (b) Same as (a) but for $\sigma$. (c) Same as (a) but for a two temperature photon distribution with an intense low energy component. (d) Same as (c) but for $\sigma$.

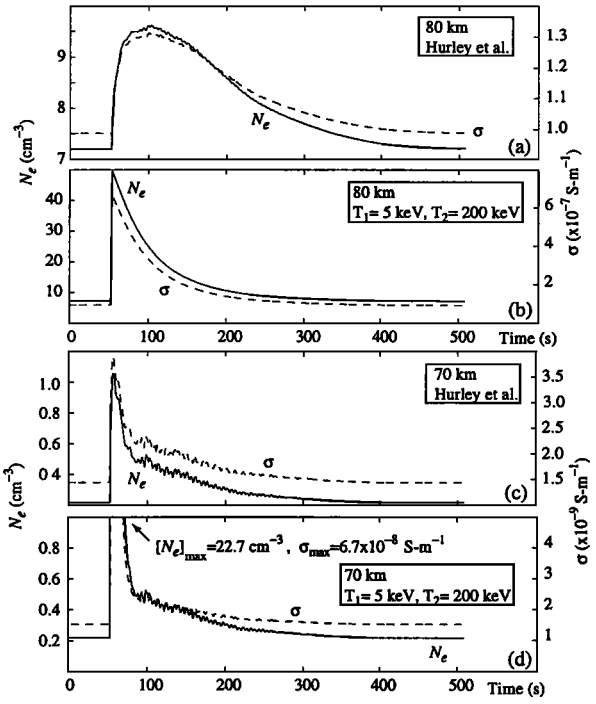


**Figure 6.** (a) Time profile of $N_e$ and $\sigma$ at 80 km calculated with a Monte Carlo model, for the photon flux-time-energy distribution given by *Hurley et al.*, 1999]. (b) Same as (a) but for a two temperature photon distribution with an intense low energy component. (c) Same as (a) for 70 km altitude. (d) Same as (c) but for 70 km altitude.

To explain the relatively sharp and large VLF signal changes, we hypothesize that the giant flare from SGR 1900+14 was accompanied by a low energy <10 keV component, outside the range of the Ulysses instrument. Figures 5c and 5d show altitude profiles of $N_e$ and $\sigma$ for such a hypothesized two-temperature initial (first second of the flare) photon distribution $f(\mathcal{E}) = [\Phi_E w_1/(\mathcal{E}T_1)]e^{-\mathcal{E}/T_1} + [\Phi_E w_2/(\mathcal{E}T_2)]e^{-\mathcal{E}/T_2}$ where $w_1$ and $w_2$ are the respective weights of the components with temperatures $T_1$ and $T_2$, with the case shown corresponding to $w_1 = 0.9$, $T_1 = 5$ keV and $w_2 = 0.1$, $T_2 = 200$ keV. We choose $T_1 = 5$ keV since the peak energy deposition rate for 5 keV photons is in the important range of 70–80 km, whereas those for 3 keV and 10 keV are respectively at ~82 km and 60 km. The $f(\mathcal{E})$ after the first second of the flare was taken to be a single temperature distribution with $T = 30$ keV. The corresponding $N_e$

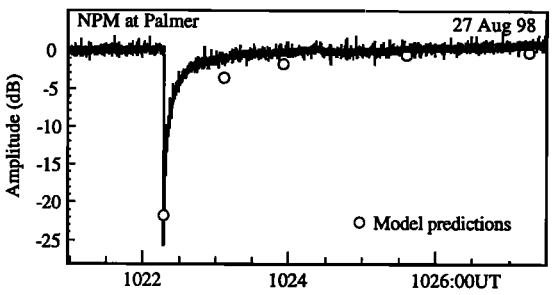


**Figure 7.** Observed NPM–PA amplitude in comparison with values (open circles) calculated using the VLF propagation model for the profiles of Figure 5c and 5d.

and $\sigma$ at 80 and 70 km altitudes (Figure 6b and 6d) now exhibit sharp onsets, and $\Delta N_e$ and $\Delta\sigma$ are much larger, and recover back to ambient levels within <200 s, as observed.

**VLF Propagation Model Calculations.** We use a VLF earth-ionosphere waveguide propagation model [*Lev-Tov et al.*, 1996, and references therein] to determine the amplitude of the NPM–PA signal at different times with respect to the event onset ($t = 0$). The model describes the electromagnetic fields as a sum of coupled waveguide modes, accounting for the various mode excitation factors, the nonperfectly conducting ground/sea surfaces, orientation of the earth's magnetic field, and effects of ions as well as electrons. The model input is the altitude profile of $N_e$ (and thus $\sigma$) calculated using the Monte Carlo model at different points along the NPM–PA path as a function of $\psi$ and time. We model the NPM–PA signal in view of the relatively simple mode structure of this all-sea-based path [*Inan and Carpenter*, 1987; *Lev-Tov et al.*, 1996].

For the single temperature incident photon distribution of *Hurley et al.* [1999], calculations indicate a peak ($t = 0^+$) amplitude change $[\Delta A]_{\max} \simeq -2.8$ dB, nearly a factor of ten smaller than the observed ~24 dB. On the other hand, we find $[\Delta A]_{\max} \simeq -22$ dB for the case of the hypothesized initial two-temperature distribution ($w_1$=0.9, $T_1$=5 keV and $w_2$=0.1, $T_2$=200 keV). Furthermore, the calculated values for $t$=50,100,200, and 300 s are in remarkable agreement with the data (Figure 7), suggesting that the giant flare from SGR1900+14 was indeed accompanied by a low energy component outside the range of the Ulysses instrument. Our choice of $w_1 = 0.9$ is based on a quantitative comparison of the observed and calculated peak signal changes. For example, $w_1$=$w_2$=0.5 give $[\Delta A]_{\max} \simeq -16$ dB, while $w_1$=0.7, $w_2$=0.3 gives $[\Delta A]_{\max} \simeq -20$ dB.

## 4. Summary and Discussion

The giant flare from SGR1900+14 significantly affected the lower ionosphere at altitudes <80 km, enhancing $N_e$ at 80 km by as much as 50 cm$^{-3}$, and increasing the ionospheric conductivity to near daytime levels. The VLF signals remained perturbed for ~200–300 s and exhibited a 5.16 s fluctuation. Quantitative interpretation indicates that this $\gamma$–ray flare was accompanied by a significant low energy (3–10 keV) photon component that carried substantially higher (by a factor of ~9) total energy than the energetic component measured on Ulysses by *Hurley et al.* [1999].

Our hypothesis that the ionospheric effect registered by the VLF signal is due primarily to a low energy photon component not detected on Ulysses is supported by the fact that the 'risetime' of the VLF event is different than that of the photon counts detected on the spacecraft (Figure 3). After careful consideration of the effects on the Ulysses data of a low energy component and investigation of whether other spacecraft might have directly detected such a component, we conclude that no data exist which contradict this hypothesis.

**Acknowledgments.** This research was supported by NSF (grants OPP-96115855 and ATM-9528173), by the AFGL (HAARP diagnostics contract F19628-96-C-0149), and by ONR (grant N00014-94-1-0100). K. Hurley is grateful for Ulysses support under JPL Contract 958056, and for the assistance of J. McTiernan. We gratefully acknowledge useful discussions with G. J. Fishman and thank R. W. Romani for his comments on the manuscript.

## References

Brown, R. T., Ionospheric Effects of Cosmic $\gamma$-ray Bursts, *Nature, 246*, 83, 1973.

Cummer, S. A., T. F. Bell, and U. S. Inan, VLF Remote Sensing of High-Energy Auroral Particle Precipitation, *J. Geophys. Res., 102*, 7477, 1997.

Edwards, P. J., G. J. Burtt, and F. Knox, Ionospheric Effect caused by Celestial X–rays, *Nature*, Vol. 222, p.p.1053-1054, June 14, 1969.

Fano, U., L. V. Spencer and M. J. Berger, Penetration and diffusion of x-rays. In *Encyclopedia of Physics*, v. 38/2, p. 660, Springer-Verlag, 1959.

Fishman G. J. and U. S. Inan, Observation of an ionospheric disturbance caused by a gamma–ray burst, *Nature*, Vol. 331, pp.418–420, 4 February 1988.

Goldberg, R. A., J. R. Barcus, and J. D. Mitchell, Response of the Middle Atmosphere to Sco X–1, 1985.

Heitler, W, *The Quantum Theory of Radiation, 3rd ed.*, Clarendon, Oxford, 1954.

Hubbell, J. H., *Photon Cross Sections, Attenuation Coefficients, and Energy Absorption Coefficients From 10 keV to 100 GeV*. US Dept. of Commerce Publ. NSRDS-NBS, *29*, 1969.

Hurley, K., T. Cline, E. Mazets, S. Barthelmy, P. Butterworth, F. Marshall, D. Palmer, R. Aptekar, S. Golenetskii, V. Il'inski, D. Frederiks, J. McTiernan, R. Gold and J. Trombka, A giant periodic flare from the soft $\gamma$-ray repeater SGR1900+14, *Nature, 397*, p. 41, January 1999.

Inan, U. S. and D. L. Carpenter, Lightning-induced electron precipitation events observed at $L$ ~2.4 as Phase and Amplitude Perturbations on Subionospheric VLF Signals, *J. Geophys. Res.*, Vol. 92, No. A4, p. 3293, 1987.

Inan, U. S., A. Slingeland, V. P. Pasko, and J. V. Rodriguez, VLF and LF signatures of mesospheric/lower ionospheric response to lightning discharges, *J. Geophys. Res., 101*, 5219-5238, 1996.

Lev-Tov, S. J., U. S. Inan, A. J. Smith, and M. A. Clilverd, Characteristics of localized ionospheric disturbances inferred from VLF measurements at two closely spaced receivers, *J. Geophys. Res., 101*, 15,737, 1996.

Pasko, V. P., and U. S. Inan, Recovery signatures of lightning-associated VLF perturbations as a measure of the lower ionosphere, *J. Geophys. Res., 99*, 17523, 1994.

Rees, M. H., Auroral ionization and excitation by incident energetic electrons, *Planet. Space Sci., 11*, 1209, 1963.

Storm, E. and H. I. Israel, Photon Cross Sections From 1 keV to 100 MeV for Elements $Z = 1$ to $Z = 100$, *Nuclear Data Tables, A7*, 565, 1970.

U. S. Inan, N. G. Lehtinen, S. J. Lev-Tov, M. P. Johnson, T. F. Bell, STAR Laboratory, Stanford University, Stanford, CA 94305

K. Hurley, UC Berkeley Space Sciences Laboratory, Berkeley, CA 94720-7450

(Received June 6, 1999; accepted July 8, 1999.)